Editors' Suggestion

Native point defects and impurities in hexagonal boron nitride

L. Weston,[1] D. Wickramaratne,[1] M. Mackoit,[2] A. Alkauskas,[2] and C. G. Van de Walle[1]
[1]*Materials Department, University of California, Santa Barbara, California 93106-5050, USA*
[2]*Center for Physical Sciences and Technology, Vilnius LT-10257, Lithuania*

(Received 17 January 2018; published 18 June 2018)

Hexagonal BN (*h*-BN) is attracting a lot of attention for two-dimensional electronics and as a host for single-photon emitters. We study the properties of native defects and impurities in *h*-BN using density functional theory with a hybrid functional. Native vacancy and antisite defects have high formation energies, and are unlikely to form under thermodynamic equilibrium for typical growth conditions. Self-interstitials can have low formation energies when the Fermi level is near the band edges, and may form as charge compensating centers; however, their low migration barriers render them highly mobile, and they are unlikely to be present as isolated defects. The defect chemistry of *h*-BN is most likely dominated by defects involving carbon, oxygen, and hydrogen impurities. Substitutional carbon and oxygen, as well as interstitial hydrogen and boron vacancy–hydrogen complexes, are low-energy defects in *h*-BN. Based on our results, we can rule out several proposed sources for defect-related luminescence in *h*-BN. In particular, we find that the frequently observed 4.1 eV emission cannot be associated with recombination at C_N, as has been commonly assumed. We suggest alternative assignments for the origins of this emission, with C_B as a candidate. We also discuss possible defect origins for the recently observed single-photon emission in *h*-BN, identifying interstitials or their complexes as plausible centers.

DOI: 10.1103/PhysRevB.97.214104

I. INTRODUCTION

Hexagonal boron nitride (*h*-BN) is an sp^2-bonded layered van der Waals material with a structure similar to graphite—or, in monolayer form, similar to graphene. *h*-BN shows excellent chemical and thermal stability. Due to the excellent lattice match with graphene, it is widely used as a dielectric and substrate for two-dimensional electronics [1–3]. It is now well established that *h*-BN has an optical band gap of 6.08 eV [4], and recent advances in single crystal [5], as well as in mono- and multilayer growth [6–8], have led to a flurry of research on *h*-BN as a potential material for wide-band-gap electronic and optoelectronic applications [4,9–11].

Photoluminescence measurements have shown that *h*-BN exhibits bright excitonic luminescence in the deep ultraviolet [5]. In addition, *h*-BN exhibits a rich array of sub-band-gap luminescence lines originating from recombination at point defects, i.e., native defects or impurities [12]. Point defects can have a profound impact on the electronic and optical properties of semiconductors [13], and their characterization is fundamental to understanding materials properties. Point defects may act as compensating centers that interfere with achieving *n*-type or *p*-type conductivity. For *h*-BN, there have been very few reports of *n*-type or *p*-type doping [14,15], and high quality doping (with large carrier concentrations and high mobility), has not been reproducibly achieved. Point defects can also act as recombination centers (both radiative and nonradiative), reducing the efficiency of band-gap luminescence [16].

As-grown *h*-BN frequently exhibits deep-level luminescence with a zero-phonon line (ZPL) at 4.1 eV [17–21] and relatively weak coupling to bulk phonon modes (Huang-Rhys factor $S = 1.3$ [19]). This emission has typically been associated with the acceptor level of a C impurity substituting for a lattice N atom (C_N) [17,20]. Recently, the 4.1 eV luminescence has been shown to exhibit single-photon emission (SPE) [22]. In a series of papers, Tran *et al.* also identified SPE from color centers in irradiated or annealed *h*-BN emitting at energies between 1.6 and 2.2 eV [11,23,24]. Subsequent experiments have reported a broad range of color centers exhibiting SPE with ZPLs in this energy range and widely varying vibronic properties [25–27]. These results highlight the potential of *h*-BN for applications related to quantum information science, including quantum computing and quantum-secure communication.

Despite the obvious technological importance, the precise chemical nature of the dominant point defects in *h*-BN remains unclear, as this is extremely difficult to characterize experimentally. First-principles calculations can play a crucial role in identifying the dominant defects, and providing accurate information about their electronic and optical properties. In recent years, advanced calculations based on hybrid density functional theory have provided considerable insight into the defect properties of III-nitrides [28–30]. A number of previous studies have addressed native point defects or impurities in *h*-BN using first-principles calculations [31–36]. However, these studies all had shortcomings, such as being based on less accurate functionals, not considering all possible spin configurations, or not including proper finite-cell-size corrections (the latter being very important for the energetics of charged defects). As such, an accurate and comprehensive picture of the defect chemistry in *h*-BN is still not available.

In this paper, we study the electronic and energetic properties of native point defects and selected impurities in *h*-BN. We use a hybrid functional, which provides an accurate band structure for the host, as well as a reliable description of carrier localization, ensuring a correct treatment of defect physics [37]. We also investigate the migration properties of

 ©2018 American Physical Society

these point defects to determine their kinetics at different temperatures. We find that isolated vacancies and antisites have very high formation energies and are unlikely to form in large concentrations in as-grown materials. Interstitials can have low formation energies under certain chemical environments, however, they are too mobile to be stable as isolated defects, even at room temperature; these defects may be present in the form of complexes. In addition to native defects, we have studied carbon, oxygen, and hydrogen impurities in h-BN, as these elements tend to be present in the growth environment. These impurities can have low formation energies and may be present in significant concentrations in nominally undoped h-BN.

We will discuss the calculated electronic and optical properties of native defects and impurities in light of experimental work. We are able to rule out the common attribution of the 4.1 eV luminescence to C_N, and identify plausible defects that may lead to the luminescence lines in the range of 1.6–2.2 eV on the basis of our calculated ZPLs.

The paper is laid out as follows: an overview of our methodology is given in Sec. II. Section III contains our results for native defects (Sec. III B) and impurities (Sec. III C). In Sec. IV, we present a comparison with experimental results. The key findings are summarized in Sec. V.

II. METHODOLOGY

A. Computational details

Our calculations are performed using density functional theory (DFT) within the generalized Kohn-Sham scheme [38]. We use the screened hybrid functional of Heyd, Scuseria, and Ernzerhof (HSE) [39,40]. In this approach, the short-range exchange potential is calculated by mixing a fraction of nonlocal Hartree-Fock exchange with the generalized gradient approximation of Perdew, Burke, and Ernzerhof (PBE) [41]. The screening parameter is set to 0.2 $Å^{-1}$ and the mixing parameter to $\alpha = 0.31$. As will be shown in Sec. III A, this value of α closely reproduces the experimental band gap and structural parameters of h-BN. This value of α is similar to what has been used to study GaN and AlN [42]. A correction for the van der Waals interactions is included within the Grimme-D2 scheme [43].

The valence electrons are separated from the core by use of projector augmented wave (PAW) potentials [44] as implemented in the VASP code [45]. For the present calculations, B $2s^22p^1$, N $2s^22p^3$, C $2s^22p^2$, O $2s^22p^4$, and H $1s^1$ electrons are treated as valence. For the bulk h-BN primitive cell, we use a $9\times9\times3$ k-point grid for integrations over the Brillouin zone; for the larger supercells, we use a reciprocal space grid of a similar density. An energy cutoff of 500 eV is used for the plane-wave basis set. Spin polarization was taken into account.

The supercell is constructed by a change of basis to an orthorhombic structure, for which the unit cell is a rectangular prism with side lengths $a\times\sqrt{3}/2a\times c$ in terms of the length of the h-BN lattice parameters. The supercell is then a $5\times6\times2$ multiple of this orthorhombic cell, leading to a 240-atom supercell. The supercell lattice vectors are fixed to the HSE-calculated equilibrium values. Native defects and impurities are created by adding and removing atoms from the supercell, and the internal coordinates are relaxed until all forces are less than 0.01 eV/Å. To determine defect migration barriers, we use the climbing-image nudged-elastic-band method [46,47].

B. Defect calculations

We use established methodologies for evaluating defect formation energies and transition levels based on total energy calculations within the supercell approach [37,48]. For a defect D with charge state q, the formation energy $E^f[D^q]$ is calculated as

$$E^f[D^q] = E_{\text{tot}}[D^q] - E_{\text{tot}}[h\text{-BN}] - \sum_i n_i\mu_i + q\,E_F + \Delta^q, \quad (1)$$

where $E_{\text{tot}}[D^q]$ is the total energy of the supercell containing D^q, and $E_{\text{tot}}[h\text{-BN}]$ is the total energy of the defect-free supercell. n_i represents the number of atoms of type i that are added ($n > 0$) or removed ($n < 0$), and the chemical potential μ_i represents the energy of the reservoir with which the atomic species are exchanged. The electron chemical potential is given by the position of the Fermi level (E_F), taken with respect to the valence-band maximum (VBM). Finally, Δ^q is a charge-state dependent term that corrects for the finite size of the supercell [49,50].

The defect charge-state transition level $\varepsilon(q/q')$ is defined as the Fermi-level position below which the defect is stable in charge state q, and above which it is stable in charge state q'. It is calculated as

$$\varepsilon(q/q') = \frac{E^f(D^q; E_F = 0) - E^f(D^{q'}; E_F = 0)}{q' - q}, \quad (2)$$

where $E^f(D^q; E_F = 0)$ is the formation energy of D^q when the Fermi level is at the VBM (i.e., for $E_F = 0$).

C. Chemical potentials

The chemical potentials μ_i are variables that represent experimental conditions. For the calculations in this work, μ_B is referenced to the total energy of a single atom in solid-phase B, and μ_N is referenced to the total energy of a N atom in a N_2 molecule; we define $\Delta\mu_N$ and $\Delta\mu_B$ with respect to these energies. Bounds are placed on the $\Delta\mu$ values based on the stability condition for h-BN. In thermodynamic equilibrium,

$$\Delta\mu_B + \Delta\mu_N = \Delta H_f(\text{BN}), \quad (3)$$

where $\Delta H_f(\text{BN})$ is the enthalpy of formation for BN. Equilibrium with N_2 sets an upper bound on μ_N (N-rich conditions): $\Delta\mu_N = 0$. Equation (3) then yields $\Delta\mu_B = \Delta H_f(\text{BN})$ in the N-rich limit. We can also define an N-poor limit, with $\Delta\mu_N = \Delta H_f(\text{BN})$ and $\Delta\mu_B = 0$. The HSE-calculated value for $\Delta H_f(\text{BN})$ is -2.90 eV, in reasonable agreement with the experimental value of -2.6 eV [51]. Neither N-rich nor N-poor conditions realistically represent actual growth conditions, but they serve as limiting cases.

We also assign chemical potentials to the C, H, and O impurity species. μ_C is referenced to the total energy of a C atom in diamond. For μ_H and μ_O, the diatomic molecules H_2 and O_2 are used as a reference. The high stability of B_2O_3 imposes an additional upper bound on

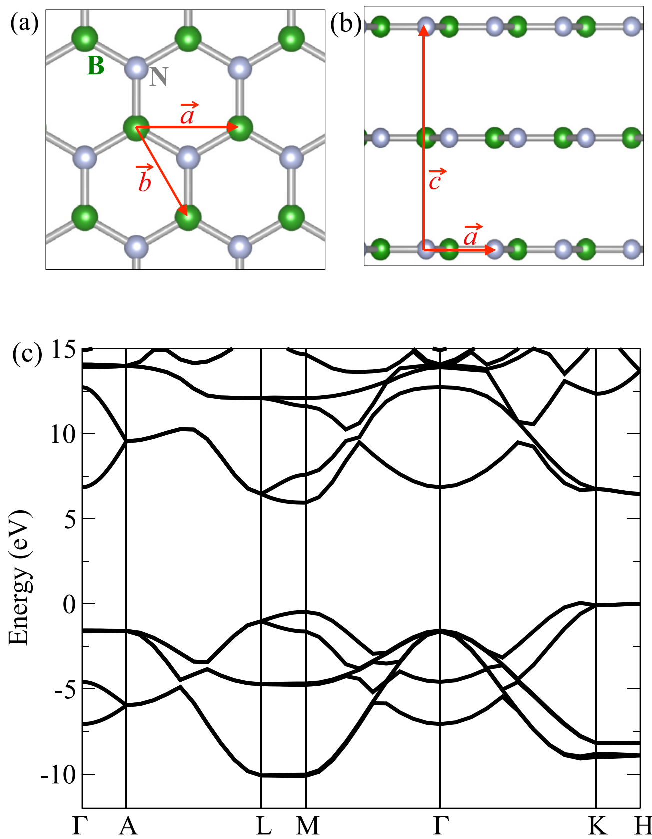

FIG. 1. (a) Top-down view of the in-plane honeycomb structure of h-BN. Boron atoms are indicated by green spheres, nitrogen are grey. (b) Side view showing the interlayer spacing and AA′ stacking sequence. (c) Electronic band structure plotted along a high-symmetry path in the Brillouin zone. The energy of the highest occupied valence state is set to zero.

$\mu_{\rm O}$: $2\Delta\mu_{\rm B} + 3\Delta\mu_{\rm O} \leqslant \Delta H_f(\rm B_2O_3)$, where we have calculated $\Delta H_f(\rm B_2O_3) = -12.69$ eV.

III. RESULTS

A. Bulk properties

The bulk crystal structure of h-BN is shown in Figs. 1(a) and 1(b); the symmetry of the crystal has a space group P6_3/mmc and point group D_{6h}. Within the (0001) plane, each nitrogen atom is threefold coordinated to boron and *vice versa*, in a honeycomb pattern that is a result of sp^2 bonding. The in-plane B–N bond length is calculated to be 1.44 Å. Out of the plane, h-BN exhibits AA′-type stacking with alternating B and N atoms along the [0001] direction. The interlayer separation is determined by the van der Waals interaction and calculated to be 3.28 Å. In Table I, the calculated lattice parameters are compared with experiment. The experimental geometry is clearly very well reproduced within our first-principles calculations.

The calculated electronic band structure for h-BN is plotted in Fig. 1(c). The valence-band maximum (VBM) is derived from π-bonding states with mostly N $2p_z$ character; the conduction-band minimum (CBM) is derived from π^*-antibonding states with mostly B $2p_z$ character. The VBM is found at the so-called T_1 point near K (between Γ and K); the CBM is at the M point. The indirect fundamental band gap is 5.94 eV; the lowest direct gap is 6.42 eV at the M point. As shown in Table I, the calculated fundamental indirect band gap is close to the experimental value of 6.08 eV [4]. The HSE calculated band gaps are also in agreement with the quasiparticle gaps of Arnaud *et al.* based on GW calculations [53].

TABLE I. Calculated bulk properties of h-BN. Experimental values are listed for comparison.

	Present	Exp.
a (Å)	2.49	2.50 [52]
c (Å)	6.55	6.65 [52]
$E_g^{\rm ind}$ (eV)	5.94	6.08 [4]
$E_g^{\rm dir}$ (eV)	6.42	

B. Native point defects in *h*-BN

Below we present results for the electronic, energetic, and migration properties of native point defects in h-BN. Because results for geometries of native defects have been reported previously [32,34,54], we do not include them in the main text. For completeness, information about the native-defect geometries is included in Ref. [55] (Sec. S1).

1. Electronic properties

Boron vacancy ($V_{\rm B}$). Each boron in the h-BN lattice has three nearest-neighbor nitrogen atoms. Removing the boron atom leaves three N $2sp^2$ and three N $2p_z$ dangling bonds. These dangling bonds combine to form localized symmetric (a^σ, a^π) and higher-lying antisymmetric (e^σ, e^π) molecular orbitals. The defect states of $V_{\rm B}$ are largely derived from valence-band orbitals. Electron counting indicates that the defect can accept up to three electrons, i.e., $V_{\rm B}$ is in principle a triple acceptor. In the neutral charge state, three holes appear in the high-lying e states of the minority spin channel, corresponding to a high-spin (HS) $S = 3/2$ paramagnetic state. $V_{\rm B}$ was previously reported to possess a low spin (LS) ground state, based on calculations within the local density approximation (LDA) [56]; in our HSE calculations (which treat exchange more accurately, particularly for highly localized states [57]), the HS–LS energy splitting is 0.8 eV, showing the HS state is strongly favored.

The charge-state transition levels are plotted in Fig. 2. When the Fermi level is near the VBM, $V_{\rm B}$ is stable in the neutral charge state. With increasing Fermi level, $V_{\rm B}$ transitions into a 1− charge state; for yet higher values of the Fermi level, the 2− charge state is stabilized. The transition levels are all found at a large energy from the VBM, making $V_{\rm B}$ a very deep acceptor. The 3− charge state is found not to be stable.

Nitrogen vacancy ($V_{\rm N}$). The removal of a N atom from the h-BN lattice leaves three B $2sp^2$ and three B $2p_z$ dangling bonds and, as with $V_{\rm B}$, these combine into low-lying a states and higher-lying e states. The $V_{\rm N}$ defect states are largely derived from conduction-band orbitals. Electron counting indicates that in the neutral charge state, three electrons occupy the

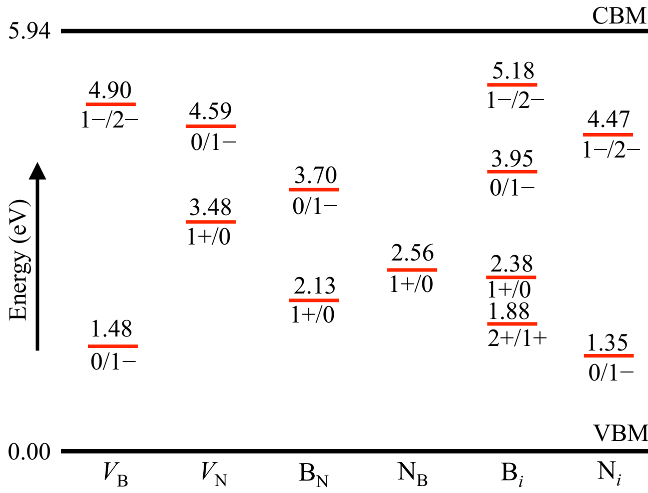

FIG. 2. Charge-state transition levels [Eq. (2)] for point defects in h-BN.

lowest a defect orbitals. In the neutral charge state, there exists only one gap state that is singly occupied, with $S = 1/2$. This state can therefore either donate or accept a single electron; V_N acts as both a donor and an acceptor. As shown in Fig. 2, the $\varepsilon(1+/0)$ and $\varepsilon(0/1-)$ levels of V_N lie deep in the band gap. Both the 1+ and 1− charge states are nonmagnetic.

Boron antisite (B_N). A boron atom can substitute for a lattice N atom to form an antisite defect B_N. In this case, gap states form from the localized B–B bonds. Boron has two fewer valence electrons than nitrogen, so in the neutral charge state this defect introduces two holes, both of which occupy the highest defect state, resulting in a nonmagnetic ground state ($S = 0$). As neutral B_N introduces occupied and unoccupied gap states, this defect can act as both a single donor and acceptor, with higher charge states not being stable. The $\varepsilon(1+/0)$ and $\varepsilon(0/1-)$ levels are indicated in Fig. 2. Both the 1+ and 1− charge states have $S = 1/2$.

Nitrogen antisite (N_B). The N_B defect forms when a N atom substitutes for a lattice B atom, leading to the formation of N–N bonds. The N atom has two extra valence electrons when compared to B, and these electrons fill the lowest unoccupied N_B defect state in a nonmagnetic ($S = 0$) configuration. Removing an electron from this defect orbital results in a positively charged state with $S = 1/2$. We find that a 2+ state is never stable. The $\varepsilon(1+/0)$ level occurs around midgap, at 2.56 eV (Fig. 2).

Boron interstitial (B_i). Given the layered nature of h-BN, the interstitial is essentially intercalated. When a B atom is present at the intercalated site, a large number of gap states associated with the atomic levels of the B atom appear. The B_i defect can act as a donor, with the 1+ and 2+ charge states becoming stable when the Fermi level moves closer to the VBM. B_i can also act as an acceptor when the Fermi level is closer to the CBM, stabilizing the 1− and 2− charge states. All of the charge-state transition levels for B_i are presented in Fig. 2.

Nitrogen interstitial (N_i). Unlike B_i, which forms at an intercalated site, N_i prefers to incorporate in a split-interstitial configuration, in which it forms a covalent bond with a lattice N atom. The end result is similar to a N_2 molecule substituting on a N site. This defect introduces unoccupied gap states, which are essentially the antibonding states of the N_2 molecule; consequently, N_i behaves as an acceptor, with 1− and 2− charge states being stable. A positive charge state for this defect was not stable.

2. Formation energies

The formation energies for native point defects in h-BN are plotted in Fig. 3, for chemical potentials corresponding to N-rich and N-poor conditions, as detailed in Sec. II C. In thermodynamic equilibrium, the concentration of a defect (c) is determined by the formation energy according to a Boltzmann expression:

$$c = N_{\text{sites}} \exp\left(-\frac{E^f[D]}{k_B T}\right), \tag{4}$$

where N_{sites} is the concentration of sites on which the defect can form ($N_{\text{sites}} = 5.7\times10^{22}$ cm^{-3} for substitutional sites), $E^f[D]$ is the formation energy [Eq. (1)], k_B is the Boltzmann constant, and T is the temperature. If conditions are close to equilibrium

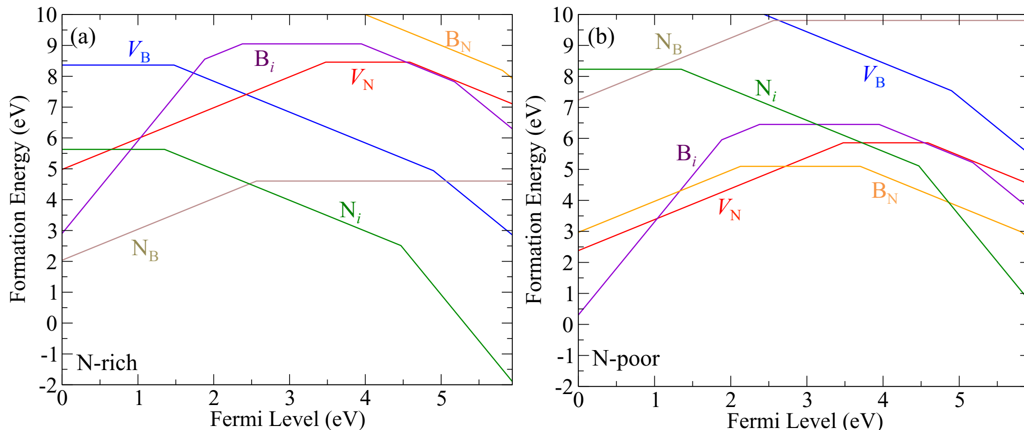

FIG. 3. Formation energies of native point defects in h-BN as a function of Fermi level under (a) N-rich and (b) N-poor conditions. The slope of each line segment corresponds to the charge state according to Eq. (1). Kinks in the curve correspond to to charge-state transition levels [Eq. (2) and Fig. 2].

(which is the case in high-temperature growth or annealing), only defects with a sufficiently low formation energy will be present in large concentrations. For the sake of our arguments, we consider temperatures in the range 700–1300 K, which are typical for chemical vapor deposition of h-BN [7,8,24]. Bulk growth is performed at higher temperatures, but defect equilibria are probably established at lower temperatures during cooldown. Because of the exponential dependence on formation energy, defect concentrations are insignificant unless the formation energy is below 2.6 eV when $T = 1300$ K or below 1.4 eV when $T = 700$ K.

We first examine the case of N-rich conditions [Fig. 3(a)], where N_B and N_i have the lowest formation energies. The formation energies of these defects depend on the Fermi level; the Fermi level, in turn, is determined by charge neutrality. In the absence of any impurities, the Fermi level would be pinned at the value for which the concentrations of positively and negatively charged point defects are equal, i.e., at the crossing point in the formation-energy curves of N_B and N_i, at 2.18 eV above the VBM. At this point, the formation energy of N_B and N_i is 4.46 eV, an extremely large value leading to negligible concentrations of these defects. This implies that the Fermi level is more likely to be determined by impurities incorporated into the material; unintentional impurities will be discussed in Sec. III C. Depending on the impurity, the Fermi level would shift closer to the VBM or to the CBM, favoring either N_B or N_i (which would act as compensating centers).

For the case of N-poor conditions, the lowest energy defects are B_i, V_N, B_N, and N_i. In the absence of impurities, the Fermi level would again be pinned around mid gap, where the formation energy of the point defects is around 5 eV. Again, this indicates a negligible native defect concentration, and points to the role of impurities in determining the Fermi level.

Finally, we comment on vacancy and antisite complexes, as several authors have suggested that they play a role in the defect chemistry of h-BN [11,58]. We have calculated the formation energies of several vacancy and antisite complexes in h-BN; the results are included in Ref. [55] (Sec. S3). Zobelli *et al.* investigated V_B-V_N vacancy complexes in the context of defect migration [58]. However, we find that the neutral V_B-V_N complex has a formation energy of 10.05 eV; consideration of other charge states does not significantly lower the energy of the defect. Tran *et al.* proposed that a neutral N_B-V_N complex could act as a color center in h-BN and account for single-photon emission [11]. Again, such a complex has a very high formation energy: 8.15 eV under the most favorable combination of chemical potentials, and considering other charge states did not substantially lower the energy of the complex. We conclude that these vacancy and antisite complexes are unlikely to play a role in h-BN.

3. Defect migration

In Sec. III B 2, we found that native point defects in h-BN tend to have very high formation energies, and in the absence of impurities will not form in large concentrations under thermodynamic equilibrium. The notion of equilibrium is important in this argument, raising the question how equilibrium is achieved. The population of point defects will be in equilibrium if the relevant migration barriers are low enough

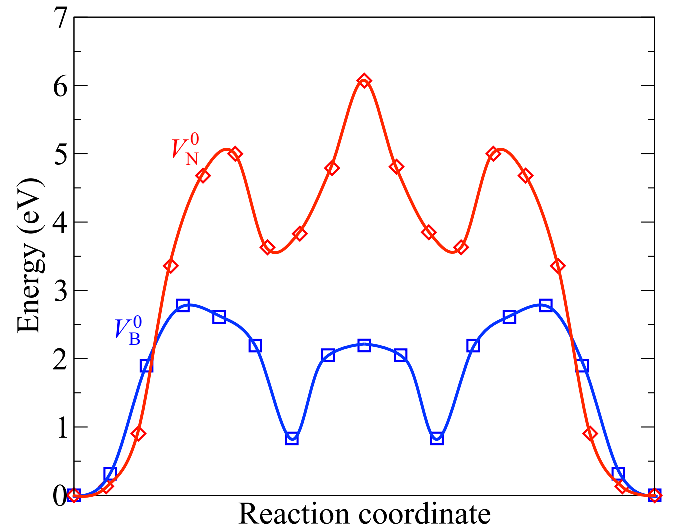

FIG. 4. Calculated potential energy surfaces for migration of the neutral boron vacancy (blue squares) and the neutral nitrogen vacancy (red diamonds) in h-BN. The curves are drawn as a guide to the eye.

to allow efficient motion of the defects at a given temperature. By determining the migration barrier (E_b) for a native point defect, we can estimate the temperature at which the defect becomes mobile; above this temperature, the system can then be considered to be in equilibrium (at least with respect to that particular defect), since it would not be possible to maintain a nonequilibrium concentration of the defect. Knowledge of this "annealing temperature" is useful for various purposes. It allows assessing whether a given growth temperature is high enough for the assumption of thermodynamic equilibrium to be valid in the determination of point-defect concentrations. In situations where nonequilibrium concentrations of point defects might be present (for instance, due to low-temperature growth, or due to intentional damage caused by, e.g., irradiation), the annealing temperature indicates at what temperature the point-defect concentration would return to equilibrium.

Within transition state theory [59], the rate Γ at which a defect hops to a neighboring equivalent site can be expressed as

$$\Gamma = \Gamma_0 \exp\left(-\frac{E_b}{k_B T}\right). \tag{5}$$

The prefactor Γ_0 is related to a typical phonon frequency; in h-BN, this can be taken as approximately 10^{14} s^{-1} [60]. An estimate for the annealing temperature can then be obtained as the temperature at which the rate $\Gamma = 1$ s^{-1} [61]. We note that the annealing temperature is not very sensitive to the choice of phonon frequency used as the prefactor in Eq. (5).

Vacancy migration. Our potential energy surfaces for migration of V_B and V_N in the neutral charge state, calculated using the climbing-image nudged-elastic-band method [46,47], are shown in Fig. 4. The paths and migration barriers for the neutral charge state are similar to those reported by Zobelli *et al.* [58]. Here we have extended the migration study to include other charge states of the vacancies. In Table II, the migration barriers for each of the stable charge states of V_B and V_N are presented, along with the annealing temperature.

TABLE II. Migration barriers (E_b) for vacancy and interstitial defects in h-BN. The charge state q is indicated, and the annealing temperature is presented, as calculated using Eq. (5) assuming a hopping rate of 1 s^{-1}.

Defect	q	E_b (eV)	Anneal T (K)
V_B	0	2.78	1000
	1−	3.09	1110
	2−	2.33	840
V_N	1+	5.51	1980
	0	5.00	1800
	1−	6.05	2180
B_i	2+	0.81	290
	1+	1.08	390
	0	0.51	180
	1−	1.05	380
	2−	0.54	190
N_i	0	0.83	300
	1−	1.00	360
	2−	0.88	320

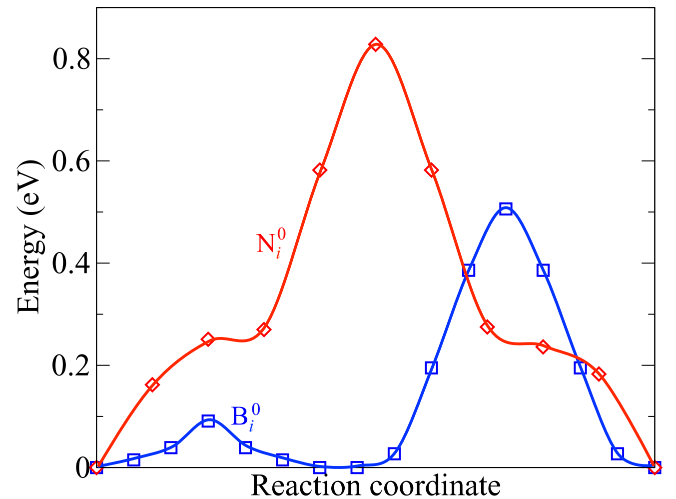

FIG. 5. Calculated potential energy surfaces for migration of the neutral boron interstitial (blue squares) and the neutral nitrogen interstitial (red diamonds) in h-BN. The curves are drawn as a guide to the eye.

For V_B, the neutral charge state has a migration barrier of 2.78 eV. There exists some variation between charge states, but E_b is relatively similar, and the annealing temperatures for these defects are around 1000 K. We can therefore assume that the concentration of V_B is likely to be in equilibrium when h-BN is grown or annealed at temperatures above 1000 K. However, V_B is "frozen in" when generated at room temperature, e.g., by electron or ion irradiation. Indeed, h-BN samples exposed to irradiation have been reported to exhibit V_B defects as well as larger V_B-related defect structures [62,63].

For V_N, the migration barriers are much larger; in the neutral charge state $E_b = 5.00$ eV. This energy corresponds to the largest barrier the defect needs to overcome along its migration path (Fig. 4). Metastable sites exist along the path, and additional barriers occur to escape out of those sites, but those intermediate barriers (on the order of 2.5 eV) are not rate limiting. The other charge states exhibit even larger barriers. These barriers are larger than vacancy migration barriers in graphite [64]; we attribute this to the need for atoms to move between second-nearest-neighbor sites in h-BN, as opposed to first-nearest-neighbor motion in graphite. Because of the high barriers, these defects do not become mobile until temperatures around 2000 K, much higher than typical growth and annealing temperatures [7,8,24], suggesting they can be present in nonequilibrium concentrations when prepared or processed under certain conditions. We note that growth of single crystals by the high-pressure high-temperature technique is performed at temperatures as high as 2000 K [5].

Interstitial migration. In Fig. 5, we plot the potential energy surfaces for migration of B_i and N_i in the neutral charge state. The stable site for intercalated B_i is just off-center from the atom above (and below) it. The small barrier in the potential energy surface is associated with a reorientation of the B atom with respect to the atoms in the surrounding layers; this barrier is easily overcome, but this step is necessary for long-range migration. The larger barrier originates from traversing the B–N bond length to a neighboring site; even the larger barrier is very low, at 0.51 eV.

For N_i, the barrier is related to breaking the N–N bond at the split-interstitial site; the N_i atom moves into the interplanar region and then to a neighboring N atom, reforming an N–N bond. The barrier for this process is again very modest, only 0.83 eV.

The migration barriers for each of the stable charge states of B_i, listed in Table II, are quite low, indicating that interstitial B atoms can move very freely in between the h-BN layers. The annealing temperatures in Table II indicate that B_i is mobile at temperatures close to room temperature. This makes it unlikely that B_i would be present as an isolated defect: B_i will move around until it is annihilated, e.g, at a vacancy or step edge, or until it can lower its energy by forming a complex with another defect. Similar arguments apply to N_i: the migration barriers are low for all charge states, and N_i is very unlikely to be present as an isolated defect.

Table II shows that, for a given defect, there is no systematic trend in migration barriers as a function of charge state. We attribute this to the fact that migration paths and barriers are governed by local bonding, which depends on the local electronic and spin state of the defect. The occupation of defect levels in the gap affects the strength of bonding, and the defects levels and the electronic structure change as the defect moves along the migration path. These properties are charge-state dependent, and hence do not necessarily follow simple trends. We have also examined migration of antisites, but all possible paths lead to very high migration barriers.

As discussed in Sec. III B 2, interstitial defects are more likely to form when the Fermi level is closer to the band edges, which would occur when dopant impurities are present. Under those conditions the interstitials will act as compensating centers, occurring in a charge state opposite to that of the dopant, and they would be Coulombically attracted to the impurities and possibly form a complex. In the next section (Sec. III C), we will discuss a number of impurities that can be unintentionally present in h-BN.

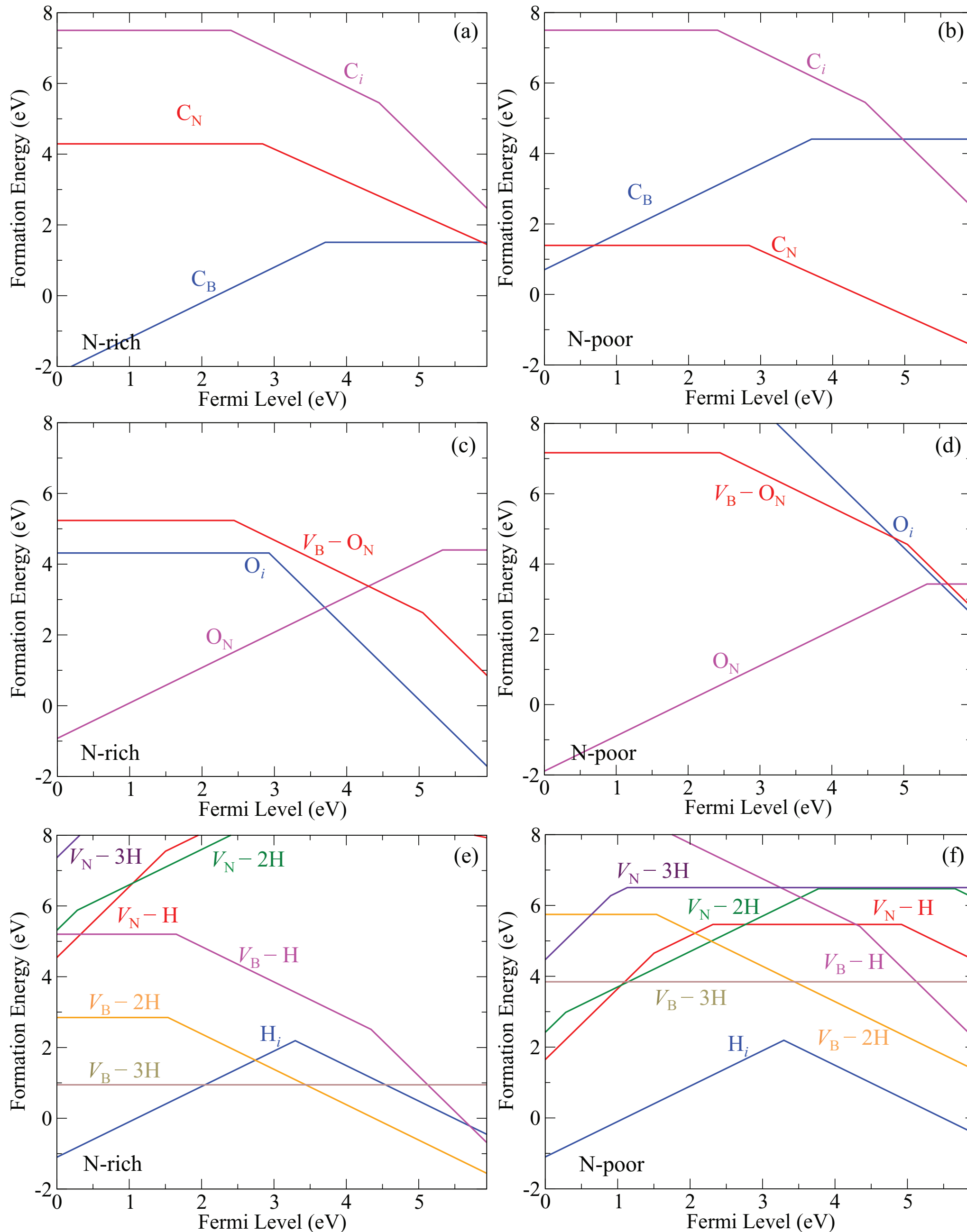

FIG. 6. Formation energies of impurity-related defect centers in *h*-BN as a function of Fermi level in N-rich and N-poor conditions for [(a) and (b)] C impurities, [(c) and (d)] O impurities, and [(e) and (f)] H impurities. The slope of each line segment corresponds to the charge state according to Eq. (1); kinks in the curves correspond to charge-state transition levels [Eq. (2)].

C. Carbon, oxygen, and hydrogen impurities in *h*-BN

As noted in Sec. III B 2, in the absence of any impurities, the native point defects in *h*-BN all have high formation energies. Impurities are therefore expected to play a dominant role in the defect chemistry. Certain impurities are likely to be present unintentionally in the growth environment, and it is important to assess whether they can be incorporated during growth. Carbon and oxygen impurities have been found to be present in III-nitrides [65–67], e.g., in GaN [68], AlN [69], as well as BN [70]. Hydrogen is also a ubiquitous impurity, and it is often part of the growth process: for growth of *h*-BN by chemical vapor deposition, hydrogen-containing precursors such as borazine ($N_3H_3B_3H_3$) [7] or ammonia borane (NH_3BH_3) [8] are used.

Our calculated formation energies for the various impurities, as well as likely complexes, are shown in Fig. 6. The charge-state transition levels are shown in Fig. 7. Comparing Fig. 6 with Fig. 3 immediately shows that impurities can have far lower formation energies than native point defects.

Below we discuss the electronic, energetic, and migration properties of these impurity-related species. The impurity geometries are presented in Ref. [55] (Sec. S2). Some of these geometries were reported previously [34,54].

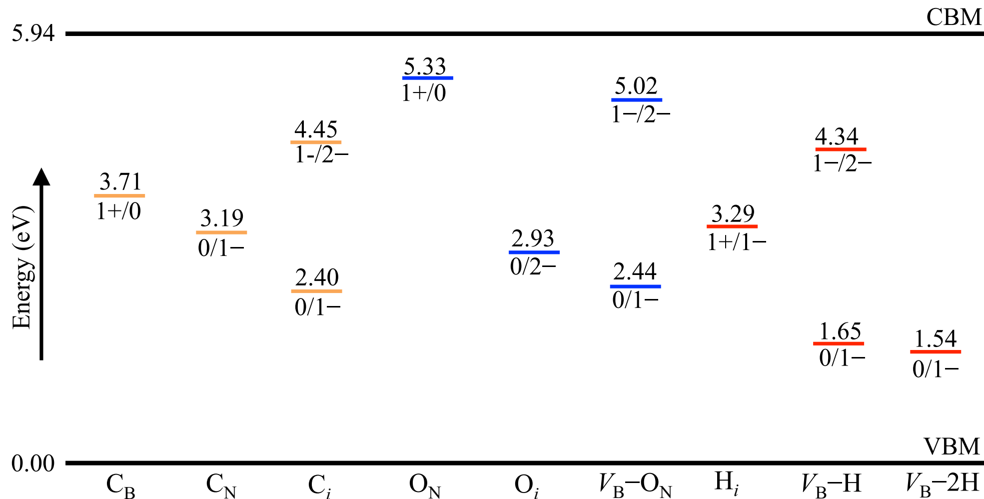

FIG. 7. Charge-state transition levels [Eq. (2)] for impurity-related defect species in *h*-BN. Defect levels related to C are shown in orange, due to oxygen in blue, and hydrogen in red.

1. Carbon

For carbon, we investigate substitution at either a B or a N site (C_B; C_N). Based on the formation energies [Figs. 6(a) and 6(b)], it is clear that substitutional carbon is easily incorporated. C_B is most favorable under N-rich conditions, and acts as a donor; the (1+/0) level is at 3.71 eV above the VBM (Fig. 7). Under N-poor conditions, C_N is dominant; this is an acceptor-type defect with a (0/1−) level 2.84 eV above the VBM.

For the case of C_B, localized C–N bonding and antibonding states form. In the neutral charge state, C_B introduces one excess electron, and this occupies an antibonding-like state in the band gap, resulting in a paramagnetic $S = 1/2$ center. The defect state is derived from C and N $2p_z$ orbitals. In the +1 charge state, C_B is nonmagnetic.

For C_N, a single hole is introduced in the neutral charge state. This hole occupies a bonding orbital with mostly C $2p_z$ character and some mixing with the surrounding B $2p_z$ states. The neutral charge state is magnetic with $S = 1/2$; the defect acts as a single acceptor, and the negative charge state is nonmagnetic.

We have also investigated an interstitial C atom (C_i). The C atom sits at an intercalated site. C_i acts as an acceptor, with a (0/1−) level 2.40 eV above the VBM, and a (1−/2−) level 4.45 eV above the VBM (Fig. 7). The formation energy of C_i is very high [Figs. 6(a) and 6(b)], and this defect is unlikely to be present in thermodynamic equilibrium; however, the migration properties of C_i are important for understanding how C impurities are incorporated unintentionally during growth, or in doping. The migration barriers are presented in Table III. The migration barrier is low for all charge states, suggesting that C_i moves freely at the intercalated site (consistent with the findings for B_i). Given the high formation energy and low migration barrier of C_i, this defect would either diffuse out of the sample, or migrate until it is annihilated by a vacancy to form C_N or C_B, or until it forms a complex with some other charged defect.

2. Oxygen

For O impurities, we consider substitution at an N site only (O_N); oxygen on the boron site (O_B) has an extremely large formation energy. The formation energies [Figs. 6(c) and 6(d)] indicate that O_N can easily incorporate, particularly under N-poor conditions, and this defect could be present in large concentrations. O_N is a deep donor, with an (1 + /0) level 5.33 eV above the VBM (Fig. 7).

For O_N, localized B–O defect states form; in the neutral charge state, an excess electron is introduced, which occupies an antibonding-like gap state with O and B $2p_z$ orbital character. Since the gap state is singly occupied, O_N^0 is paramagnetic with $S = 1/2$. The +1 charge state is nonmagnetic.

Since O_N acts as a donor, it will shift the Fermi level towards the CBM, and lower the formation energy of native defects with acceptor character. In addition, complex formation between the donor and acceptor may occur. In particular, we have explored a complex between O_N and V_B [included in Figs. 6(c) and 6(d)]; this V_B-O_N complex could be considered an analog to the N_C-V_C center in diamond. This defect acts as a deep acceptor, but its formation energy is high. In the neutral charge state, V_B-O_N has two unoccupied gap states in the minority spin channel, and prefers a HS state with $S = 1$; the defect can accept up to two electrons.

Oxygen impurities can also incorporate as an interstitial (O_i), between the *h*-BN layers. O_i acts as a double acceptor, with a (0/2−) level 2.93 eV above the VBM (Fig. 7). The

TABLE III. Migration barriers (E_b) for interstitial impurities in *h*-BN. The charge state q is indicated, and the annealing temperature is presented, as calculated using Eq. (5) assuming a hopping rate of 1 s^{-1}.

Defect	q	E_b (eV)	Anneal T (K)
C_i	0	1.01	360
	1−	0.86	310
	2−	0.92	330
O_i	0	0.53	190
	2−	0.35	130
H_i	1+	0.75	270
	1−	0.46	170

1+ charge state is never stable, i.e., O_i behaves as a "negative-U" center. The formation energy is lowest under N-rich conditions. The difference between N-rich and N-poor conditions arises because for the purposes of Figs. 6(c) and 6(d) we assume the oxygen chemical potential μ_O to be set at the solubility limit, which is determined by equilibrium with B_2O_3 (see Sec. II C). When oxygen is incorporated unintentionally, μ_O is probably well below this extreme limit, leading to large formation energies and relatively low concentrations of O_i in h-BN.

Still, the migration barriers for O_i are important to understand the kinetics of O incorporation; the barriers are listed in Table III. The O_i defect is highly mobile, even at room temperature, and would be very easily incorporated if its formation energy were low enough. Given its high mobility, O_i would then likely form complexes and we do not expect it to be present as an isolated defect.

3. Hydrogen

Interstitial hydrogen (H_i) is a common impurity in many semiconductors, and is typically amphoteric [71]; i.e, H_i will behave as a donor under p-type conditions, and as an acceptor under n-type conditions. We find the same behavior in h-BN [Figs. 6(e) and 6(f)]. H_i sits at an intercalated site, and has a (1+/1−) level 3.29 eV above the VBM (Fig. 7), consistent with the value found in Ref. [72]. The formation energy of H_i is low, particularly near the band edges, which suggests H_i can be incorporated easily and may behave as a charge-compensating center.

The migration properties of H_i are presented in Table III. This defect has a low migration barrier, with $E_b = 0.75$ eV for H_i^{1+}, and $E_b = 0.46$ eV for H_i^{1-}. This suggests that H_i is highly mobile, even at room temperature. We thus expect that H_i will form complexes with charged defects and impurities in h-BN.

Hydrogen atoms interact strongly with vacancy defects in III–nitrides [73]. We have therefore investigated complexes of V_B with one, two, or three hydrogen impurities (V_B-H; V_B-2H; V_B-3H). The formation energy of the V_B-H complexes can be low, and is lowest under N-rich conditions, which favor the formation of boron vacancies [Figs. 6(e) and 6(f)]. Hydrogen can also form complexes with V_N; these are all found to have very high formation energies, and they will not be discussed further here.

The singly decorated V_B-H complex behaves similar to V_B, with one of the N sp^2 dangling bonds passivated by hydrogen. V_B-H thus acts as a double acceptor. The neutral charge state is HS with $S = 1$; the 1− and 2− charge states have $S = 1/2$ and $S = 0$, respectively. The acceptor levels are deep; the (0/1−) and (1 − /2−) levels are shown in Fig. 7. In V_B-2H, two of the sp^2 dangling bonds on N atoms are passivated, and this defect acts as a single acceptor, with $S = 1/2$ in the neutral charge state. The 1− charge state is nonmagnetic. The fully passivated V_B-3H has a low formation energy of 0.95 eV under N-rich conditions, suggesting that it can be present in large concentrations. It is stable only in the neutral charge state and therefore this defect is electrically inactive.

Given that H_i and its complexes with V_B (V_B-3H, V_B-2H, and V_B-H) have low formation energies, it is important to understand how these defects interact, and what is the binding strength of hydrogen in these complexes. This is best expressed in terms of a *removal energy* E_r, as defined in Ref. [73]. The removal energy for a vacancy complex initially containing n H atoms, i.e., $n \rightarrow n-1$, is

$$E_r(n \rightarrow n-1) = -E^f[V_B - n\text{H}] + E^f[V_B - (n-1)\text{H}] + E^f[\text{H}_i]. \quad (6)$$

TABLE IV. Hydrogen removal energies E_r [Eq. (6)] from boron vacancy complexes.

Defect	q	E_r (eV)
V_B-3H	0	2.34
V_B-2H	0	2.90
	1−	5.18
V_B-H	0	3.53
	1−	5.69
	2−	4.13

The overall charge state of the complex cannot change during the removal process, because the typical time for carrier capture at a deep level [74] is much longer than the time scale on which the hydrogen motion occurs. We therefore enforce the same charge state for the initial complex and the sum of the "reaction products." Because H_i is amphoteric, in some cases more than one charge-conserving reaction pathway exists. The results listed in Table IV are for the lowest-energy pathway for each charge state of each complex.

To remove a hydrogen atom from the neutral V_B-3H complex requires $E_r = 2.34$ eV. All of the other removal processes require even higher energies. This suggests that very high temperatures would be required to dehydrogenate these vacancy complexes. Once formed, the V_B-nH complexes are therefore likely to be stable in h-BN. There is a possibility, however, that hydrogen could be removed from V_B complexes by electron irradiation; we note that irradiation is used to create SPEs in h-BN.

IV. DISCUSSION AND COMPARISON WITH EXPERIMENT

A. Prospects for *n*-type or *p*-type doping

Native point defects can act as compensating centers when intentional doping is attempted. Achieving n- and p-type doping of h-BN is an area of active experimental research [14,15,75]. For p-type doping (Fermi level close to the VBM), N_B is the lowest-energy compensating defect under N-rich conditions [Fig. 3(a)], while B_i and V_N are the lowest under N-poor conditions [Fig. 3(b)]. For n-type doping (Fermi level close to the CBM), the dominant compensating defect is N_i under both N-rich and N-poor conditions. As noted in Sec. III B 3, the interstitial defects are highly mobile; it is therefore likely that during cool down they would form a complex with the dopant impurities.

We note that unintentional impurities can also act as compensation centers. Interstitial hydrogen is amphoteric and would therefore compensate both p-type and n-type materials. The low formation energies of impurity species suggests that their concentrations would need to be controlled in order to

achieve doping. However, as has been well documented in GaN [76], hydrogen can play a beneficial role during growth of p-type material, and can be removed in a postgrowth activation anneal. Oxygen acts as a donor and would compensate p-type material; similarly, C_B acts as a compensating donor, while C_N acts as a compensating acceptor that would passivate n-type material.

Our discussion assumed that p-type and n-type doping would be feasible in h-BN, but that is by no means certain. In a recent study of candidate acceptors [77], we found that h-BN exhibits a strong tendency to form small polarons in the vicinity of acceptor impurities, which prohibits the Fermi level from moving close to the VBM. We also expect n-type doping to be very difficult, due to the energy of the CBM being very high (close to the vacuum level) on an absolute energy scale [72,78]. Indeed, we found that O_N, which would seem the best candidate for n-type doping, forms a deep level (Fig. 7). We therefore suggest that achieving actual n- or p-type doping will not be possible in h-BN.

B. X-ray measurements

A recent study by McDougall *et al.* combined experiment and DFT calculations to investigate the impact of point defects on the x-ray absorption near-edge structure (XANES) of h-BN [54]. The authors measured experimental XANES spectra for a number of different samples including sputtered films, single crystals, and powders; by comparing these results with DFT-calculated spectra for supercells containing point defects, the authors concluded that O_N, C_B, V_B-3H were the most dominant defects in these samples. These findings are in excellent agreement with our calculated results presented in Fig. 6, since we found that these defects have low formation energies and are likely to form. This experimental result is also in agreement with our key finding that impurities play the dominant role in determining defect equilibrium in h-BN, rather than native point defects.

C. 4.1 eV luminescence

Luminescence with a ZPL at 4.1 eV has been observed in bulk crystals of h-BN grown at high temperature and pressure [5] and in h-BN samples grown by chemical vapor deposition [21]. The 4.1 eV line has been observed in experiments with subband gap and above-band gap excitation [21] and is known to exhibit weak coupling to the bulk phonon modes, resulting in a low Huang-Rhys factor [21]. The emission line persists following irradiation of the h-BN samples [79]. Given the robust nature of this emission line and its presence irrespective of the growth technique, it is tempting to conclude that the origin of the 4.1 eV emission is a native point defect in h-BN.

A number of proposals have been put forth to explain the origin of this 4.1 eV line. Some of the proposals centered around the C_N acceptor; carbon is indeed likely to be present as an unintentional impurity in h-BN. Based on temperature-dependent photoluminescence experiments, Du *et al.* proposed that the 4.1 eV line originates from a donor-acceptor pair (DAP) recombination involving a shallow V_N donor and a deep C_N acceptor [20]. Katzir *et al.* proposed that the 4.1 eV emission originates from recombination of a conduction-band electron with a neutral C_N defect [17]. With regard to the DAP recombination model, our results [Fig. 2] clearly show that the donor level for V_N is deep in the gap, ruling out this model; moreover, to the best of our knowledge, no shallow donors have been identified in h-BN. Shallow-donor to deep-acceptor transitions are thus highly unlikely in h-BN. Regarding the nature of the deep acceptor, our calculations show that recombination of electrons in the conduction band with the $(0/1-)$ level of C_N gives rise to a ZPL at 3.1 eV. This is so far away from the observed 4.1 eV line that we can confidently rule out C_N as the source of the 4.1 eV emission.

While C_N cannot account for the 4.1 eV emission, we note that C_B has a (0/+) level at 3.71 eV above the VBM. Recombination with holes in the valence band would lead to a ZPL at this energy, which is not too far from the observed 4.1 eV emission. XANES measurements on powder and CVD-grown samples of h-BN have observed evidence of carbon impurities that are substituted on the boron site [54].

We can also inspect our comprehensive results on point defects and complexes to try and identify likely sources of the 4.1 eV emission. For optical transitions that involve a carrier in the valence band or conduction band (i.e., free-to-bound transitions), the ZPL is given simply by the energy difference between the defect levels in Fig. 2 and the band edge. This analysis neglects the possibility of defect-to-defect transitions. This is justified since all of the defects we have investigated in this study are deep and lead to localized wave functions. Furthermore, there is no evidence of shallow dopants in h-BN. Hence the spatial overlap between the wave functions of two defects will be low and will lead to weak transitions. We also do not consider intradefect transitions here; these transitions are beyond the scope of the present investigation, but cannot be ruled out.

We first consider the self-interstitials. B_i exhibits a $(0/1-)$ level at 3.95 eV and a $(1-/2-)$ level at 4.47 eV above the h-BN VBM. The position of these levels could make B_i a candidate for the 4.1 eV emission; however, we found that the interstitial has a very low migration barrier (Table II), making it mobile even at room temperature. Isolated B_i are thus unlikely to be present in h-BN, Complexes between B_i and impurities could in principle occur, but we note that the formation energy of B_i is very high (Fig. 3). The boron interstitial is thus not likely to be a source of the 4.1 eV emission. Nitrogen interstitials, which act as acceptors, have much lower formation energies. They are also very mobile but could form complexes with donor impurities such as O_N.

Turning to the antisites, the positions of the defect levels (Fig. 2) are such that they are unlikely to be responsible for the 4.1 eV line. In addition, both antisites have high formation energies and are therefore unlikely to be present in as-grown h-BN.

The same arguments apply to vacancies: the defect levels are such that they are unlikely to give rise to 4.1 eV emission, and they are high in energy. However, an interesting possibility arises in the case of boron vacancies: we have found that complexes between V_B and hydrogen or oxygen have low formation energies (Fig. 6). Hydrogen and oxygen are common impurities that can be unintentionally present during growth or processing. The formation energies of the complexes with hydrogen, in particular, are very low. If boron vacancies are

present in h-BN, it is likely in hydrogenated form. V_B-H has a (1−/2−) level at 4.34 eV (Fig. 7), which would give rise to emission at this energy by recombination with a hole in the VBM. V_B-H also has a (0/1−) level at 1.65 eV above the VBM; recombination with an electron in the CBM would lead to a ZPL at 4.29 eV. The V_B-2H complex has an even lower formation energy and a (0/1−) level at 1.54 eV above the VBM; recombination with an electron in the CBM would lead to a ZPL of 4.4 eV.

We have thus identified a number of candidates for the 4.1 eV emission line; explicit calculations of the luminescence line shape [80,81] will be necessary in order to establish whether these candidate centers can give rise to the type of sharp emission that is experimentally observed.

D. 2 eV luminescence

Measurements on irradiated or annealed h-BN samples have also frequently shown narrow emission lines with energies that range from 1.6 eV to 2.2 eV [27,82,83]; here, we broadly refer to these lines as the "2 eV luminescence." Emissions in this range of energies exhibit clear ZPLs and evidence of single photon emission [27]. Examining our calculated thermodynamic transition levels in Figs. 2 and 7 allows us to identify plausible defects that may give rise to a free-to-bound transition in the energy range of 1.6 eV to 2 eV.

Boron self-interstitials have a (2+/1+) level at 1.88 eV above the VBM. While this is in the range of the emission energies observed, boron interstitials are highly mobile (Sec. III B 3) and have a high formation energy. The B_N antisite has a (1+/0) level at 2.13 eV above the VBM, but again the formation energy of the boron antisite is quite large. Among vacancies, the hydrogenated boron vacancies are most likely to form. The V_B-H complex has a (0/1−) level at 1.65 eV above the VBM, and hence recombination with holes in the VBM would lead to a ZPL at that energy; the complex also has a (1−/2−) level at 4.34 eV above the VBM, for which recombination with electrons in the CBM would lead to a ZPL at 1.6 eV.

It has also been suggested that the 2 eV emission is associated with an internal transition involving an excited state of the defect [11]. Bright emission requires that the internal transition occurs between gap states in the same spin channel. We find that V_B and its complexes with hydrogen or oxygen form a high-spin state with two or more gap states in the same spin channel. We also find that interstitials that are incorporated at an intercalated site (and couple weakly to the lattice) have multiple gap states in the same spin channel. Of the interstitials we have investigated, B_i, C_i, and O_i in particular exhibit these features in their electronic structure. However, as we discuss in Sec. III, we find these defects to have low migration barriers; they are likely to be mobile at room temperature and are more likely to exist as a complex with another charged defect. It is conceivable that these complexes also exhibit multiple gap states in the same channel, which is essential for an internal transition. Defect complexes comprising multiple point defects, such as V_N-C_B [84,85], have also been suggested to give rise to multiple gap states in monolayer h-BN. None of the remaining isolated point defects that we have investigated, either native defects or impurities, exhibit multiple gap states in their electronic structure; this precludes them from being a source of the 2 eV emission due to an internal transition.

V. SUMMARY AND CONCLUSIONS

We have investigated the energetic, electronic, and migration properties of native point defects and common impurities in h-BN. Isolated native point defects in h-BN have extremely high formation energies, and in the absence of impurities are unlikely to form in observable concentrations under thermodynamic equilibrium. Interstitial defects are too mobile to be stable as isolated defects, but could be present in complexes with (intentional or unintentional) dopant impurities. Vacancy defects have much higher migration barriers and could be present in nonequilibrium conditions, for instance, after irradiation. The defect chemistry of h-BN is likely dominated by C, O, and H impurities. Complex formation with hydrogen or oxygen significantly lowers the formation energy of boron vacancies.

Based on our calculated results, we discussed mechanisms for the experimentally observed 4.1 eV and 2 eV emission lines. We can exclude C_N as a source for the 4.1 eV emission, and suggest alternative assignments, with C_B as one possibility. For SPEs around 2 eV, we propose interstitials or their complexes as plausible centers. Overall, our results provide essential information towards identifying the microscopic origin of SPE in h-BN.

Note added in proof. Recently, we became aware of questions surrounding the origins of a frequently observed luminescence signal around 5.3 eV [79,86,87]. Based on the calculated charge-state transition level of the O_N impurity (see Fig. 7) we suggest this luminescence is related to unintentionally incorporated oxygen.

ACKNOWLEDGMENTS

L.W. was supported by the National Science Foundation (NSF) MRSEC program (DMR-1720256). C.VdW. was supported by the National Science Foundation under Grant No. DMR-1434854. D.W. was supported by the U.S. Department of Energy (DOE), Office of Science, Basic Energy Sciences (BES) under Award No. DE-SC0010689. Computational resources were provided by the Center for Scientific Computing at the CNSI and MRL (an NSF MRSEC, DMR-1720256) (NSF CNS-0960316), and by the Extreme Science and Engineering Discovery Environment (XSEDE), supported by the NSF (ACI-1548562). A.A. and M.M. acknowledge the support of the Research Council of Lithuania via Grant No. M-ERA.NET-1/2015, as well as computational resources at the High Performance Computing Center "HPC Sauletekis" (Physics Department, Vilnius University).

[1] C. R. Dean, A. F. Young, I. Meric, C. Lee, L. Wang, S. Sorgenfrei, K. Watanabe, T. Taniguchi, P. Kim, K. Shepard, and J. Hone, Nat. Nanotechnol. **5**, 722 (2010).

[2] J. Xue, J. Sanchez-Yamagishi, D. Bulmash, P. Jacquod, A. Deshpande, K. Watanabe, T. Taniguchi, P. Jarillo-Herrero, and B. J. LeRoy, Nat. Mater. **10**, 282 (2011).

[3] M. Yankowitz, J. Xue, D. Cormode, J. D. Sanchez-Yamagishi, K. Watanabe, T. Taniguchi, P. Jarillo-Herrero, P. Jacquod, and B. J. LeRoy, Nat. Phys. **8**, 382 (2012).
[4] G. Cassabois, P. Valvin, and B. Gil, Nat. Photon. **10**, 262 (2016).
[5] K. Watanabe, T. Taniguchi, and H. Kanda, Nat. Mater. **3**, 404 (2004).
[6] K. K. Kim, A. Hsu, X. Jia, S. M. Kim, Y. Shi, M. Hofmann, D. Nezich, J. F. Rodriguez-Nieva, M. Dresselhaus, T. Palacios, and J. Kong, Nano Lett. **12**, 161 (2011).
[7] Y. Shi, C. Hamsen, X. Jia, K. K. Kim, A. Reina, M. Hofmann, A. L. Hsu, K. Zhang, H. Li, Z.-Y. Juang, M. S. Dresselhaus, L.-J. Li, and J. Kong, Nano Lett. **10**, 4134 (2010).
[8] L. Song, L. Ci, H. Lu, P. B. Sorokin, C. Jin, J. Ni, A. G. Kvashnin, D. G. Kvashnin, J. Lou, B. I. Yakobson, and P. M. Ajayan, Nano Lett. **10**, 3209 (2010).
[9] Y. Kubota, K. Watanabe, O. Tsuda, and T. Taniguchi, Science **317**, 932 (2007).
[10] K. Watanabe, T. Taniguchi, T. Niiyama, K. Miya, and M. Taniguchi, Nat. Photon. **3**, 591 (2009).
[11] T. T. Tran, K. Bray, M. J. Ford, M. Toth, and I. Aharonovich, Nat. Nanotechnol. **11**, 37 (2016).
[12] A. Lukomskii, V. Shipilo, and L. Gameza, J. Appl. Spectrosc. **57**, 607 (1992).
[13] H. Morkoç, *Handbook of Nitride Semiconductors and Devices* (Wiley, New York, 2008), Vol. 1–3.
[14] B. He, W. Zhang, Z. Yao, Y. M. Chong, Y. Yang, Q. Ye, X. Pan, J. Zapien, I. Bello, S. Lee, I. Gerhards, H. Zutz, and H. Hofsäss, Appl. Phys. Lett. **95**, 252106 (2009).
[15] R. Dahal, J. Li, S. Majety, B. Pantha, X. Cao, J. Lin, and H. Jiang, Appl. Phys. Lett. **98**, 211110 (2011).
[16] M. A. Reshchikov and H. Morkoç, J. Appl. Phys. **97**, 061301 (2005).
[17] A. Katzir, J. Suss, A. Zunger, and A. Halperin, Phys. Rev. B **11**, 2370 (1975).
[18] M. G. Silly, P. Jaffrennou, J. Barjon, J.-S. Lauret, F. Ducastelle, A. Loiseau, E. Obraztsova, B. Attal-Tretout, and E. Rosencher, Phys. Rev. B **75**, 085205 (2007).
[19] L. Museur, D. Anglos, J.-P. Petitet, J.-P. Michel, and A. V. Kanaev, J. Lumin. **127**, 595 (2007).
[20] X. Du, J. Li, J. Lin, and H. Jiang, Appl. Phys. Lett. **106**, 021110 (2015).
[21] T. Q. P. Vuong, G. Cassabois, P. Valvin, A. Ouerghi, Y. Chassagneux, C. Voisin, and B. Gil, Phys. Rev. Lett. **117**, 097402 (2016).
[22] R. Bourrellier, S. Meuret, A. Tararan, O. Stéphan, M. Kociak, L. H. Tizei, and A. Zobelli, Nano Lett. **16**, 4317 (2016).
[23] T. T. Tran, C. Zachreson, A. M. Berhane, K. Bray, R. G. Sandstrom, L. H. Li, T. Taniguchi, K. Watanabe, I. Aharonovich, and M. Toth, Phys. Rev. Appl. **5**, 034005 (2016).
[24] T. T. Tran, C. Elbadawi, D. Totonjian, C. J. Lobo, G. Grosso, H. Moon, D. R. Englund, M. J. Ford, I. Aharonovich, and M. Toth, ACS Nano **10**, 7331 (2016).
[25] N. R. Jungwirth, B. Calderon, Y. Ji, M. G. Spencer, M. E. Flatté, and G. D. Fuchs, Nano Lett. **16**, 6052 (2016).
[26] Z. Shotan, H. Jayakumar, C. R. Considine, M. Mackoit, H. Fedder, J. Wrachtrup, A. Alkauskas, M. W. Doherty, V. M. Menon, and C. A. Meriles, ACS Photon. **3**, 2490 (2016).
[27] A. L. Exarhos, D. A. Hopper, R. R. Grote, A. Alkauskas, and L. C. Bassett, ACS Nano **11**, 3328 (2017).
[28] C. G. Van de Walle, J. L. Lyons, and A. Janotti, Phys. Status Solidi A **207**, 1024 (2010).
[29] Q. Yan, A. Janotti, M. Scheffler, and C. G. Van de Walle, Appl. Phys. Lett. **105**, 111104 (2014).
[30] J. L. Lyons and C. G. Van de Walle, NPJ Comp. Mater. **3**, 1 (2017).
[31] A. Zunger and A. Katzir, Phys. Rev. B **11**, 2378 (1975).
[32] W. Orellana and H. Chacham, Phys. Rev. B **63**, 125205 (2001).
[33] S. Azevedo, J. R. Kaschny, C. M. de Castilho, and F. de Brito Mota, Nanotechnology **18**, 495707 (2007).
[34] B. Huang and H. Lee, Phys. Rev. B **86**, 245406 (2012).
[35] V. Wang, R.-J. Liu, H.-P. He, C.-M. Yang, and L. Ma, Solid State Commun. **177**, 74 (2014).
[36] G. Cheng, Y. Zhang, L. Yan, H. Huang, Q. Huang, Y. Song, Y. Chen, and Z. Tang, Comp. Mater. Sci. **129**, 247 (2017).
[37] C. Freysoldt, B. Grabowski, T. Hickel, J. Neugebauer, G. Kresse, A. Janotti, and C. G. Van de Walle, Rev. Mod. Phys. **86**, 253 (2014).
[38] W. Kohn and L. J. Sham, Phys. Rev. **140**, A1133 (1965).
[39] J. Heyd, G. Scuseria, and M. Ernzerhof, J. Chem. Phys. **118**, 8207 (2003).
[40] J. Heyd, G. E. Scuseria, and M. Ernzerhof, J. Chem. Phys. **124**, 219906 (2006).
[41] J. P. Perdew, K. Burke, and M. Ernzerhof, Phys. Rev. Lett. **77**, 3865 (1996).
[42] P. G. Moses, M. Miao, Q. Yan, and C. G. Van de Walle, J. Chem. Phys. **134**, 084703 (2011).
[43] S. Grimme, J. Antony, S. Ehrlich, and H. Krieg, J. Chem. Phys. **132**, 154104 (2010).
[44] P. E. Blöchl, Phys. Rev. B **50**, 17953 (1994).
[45] G. Kresse and J. Furthmüller, Phys. Rev. B **54**, 11169 (1996).
[46] G. Henkelman, B. P. Uberuaga, and H. Jónsson, J. Chem. Phys. **113**, 9901 (2000).
[47] G. Henkelman and H. Jónsson, J. Chem. Phys. **113**, 9978 (2000).
[48] C. G. Van de Walle and J. Neugebauer, J. Appl. Phys. **95**, 3851 (2004).
[49] C. Freysoldt, J. Neugebauer, and C. G. Van de Walle, Phys. Rev. Lett. **102**, 016402 (2009).
[50] C. Freysoldt, J. Neugebauer, and C. G. Van de Walle, Phys. Status Solidi B **248**, 1067 (2011).
[51] I. Tomaszkiewicz, Pol. J. Chem. **76**, 891 (2002).
[52] Y. Gu, M. Zheng, Y. Liu, and Z. Xu, J. Am. Ceram. Soc. **90**, 1589 (2007).
[53] B. Arnaud, S. Lebegue, P. Rabiller, and M. Alouani, Phys. Rev. Lett. **96**, 026402 (2006).
[54] N. L. McDougall, J. G. Partridge, R. J. Nicholls, S. P. Russo, and D. G. McCulloch, Phys. Rev. B **96**, 144106 (2017).
[55] See Supplemental Material at http://link.aps.org/supplemental/10.1103/PhysRevB.97.214104 for information about the geometry of native defects (Sec. S1), the geometry of impurities (Sec. S2), and complexes between native defects (Sec. S3).
[56] C. Attaccalite, M. Bockstedte, A. Marini, A. Rubio, and L. Wirtz, Phys. Rev. B **83**, 144115 (2011).
[57] B. G. Janesko, T. M. Henderson, and G. E. Scuseria, Phys. Chem. Chem. Phys. **11**, 443 (2009).
[58] A. Zobelli, C. P. Ewels, A. Gloter, and G. Seifert, Phys. Rev. B **75**, 094104 (2007).
[59] G. H. Vineyard, J. Phys. Chem. Solids **3**, 121 (1957).
[60] R. Geick, C. Perry, and G. Rupprecht, Phys. Rev. **146**, 543 (1966).

[61] A. Janotti and C. G. Van de Walle, Phys. Rev. B **76**, 165202 (2007).
[62] C. Jin, F. Lin, K. Suenaga, and S. Iijima, Phys. Rev. Lett. **102**, 195505 (2009).
[63] L.-C. Yin, H.-M. Cheng, and R. Saito, Phys. Rev. B **81**, 153407 (2010).
[64] A. Krasheninnikov, P. Lehtinen, A. Foster, and R. Nieminen, Chem. Phys. Lett. **418**, 132 (2006).
[65] J. Neugebauer and C. G. Van de Walle, in *Advances in Solid State Physics 35* (Springer, Berlin, Heidelberg, 1996), pp. 25–44.
[66] L. Gordon, J. L. Lyons, A. Janotti, and C. G. Van de Walle, Phys. Rev. B **89**, 085204 (2014).
[67] J. L. Lyons, A. Janotti, and C. G. Van de Walle, Phys. Rev. B **89**, 035204 (2014).
[68] M. Strassburg, J. Senawiratne, N. Dietz, U. Haboeck, A. Hoffmann, V. Noveski, R. Dalmau, R. Schlesser, and Z. Sitar, J. Appl. Phys. **96**, 5870 (2004).
[69] A. Ishibashi, H. Takeishi, M. Mannoh, Y. Yabuuchi, and Y. Ban, J. Electron. Mater. **25**, 799 (1996).
[70] T. Taniguchi and K. Watanabe, J. Cryst. Growth **303**, 525 (2007).
[71] C. G. Van de Walle and J. Neugebauer, Annu. Rev. Mater. Res. **36**, 179 (2006).
[72] C. E. Dreyer, J. L. Lyons, A. Janotti, and C. G. Van de Walle, Appl. Phys. Express **7**, 031001 (2014).
[73] C. G. Van de Walle, Phys. Rev. B **56**, R10020 (1997).
[74] A. Alkauskas, Q. Yan, and C. G. Van de Walle, Phys. Rev. B **90**, 075202 (2014).
[75] S. Majety, T. Doan, J. Li, J. Lin, and H. Jiang, AIP Adv. **3**, 122116 (2013).
[76] J. Neugebauer and C. G. Van de Walle, Appl. Phys. Lett. **68**, 1829 (1996).
[77] L. Weston, D. Wickramaratne, and C. G. Van de Walle, Phys. Rev. B **96**, 100102 (2017).
[78] K. P. Loh, I. Sakaguchi, M. N. Gamo, S. Tagawa, T. Sugino, and T. Ando, Appl. Phys. Lett. **74**, 28 (1999).
[79] L. Museur, E. Feldbach, and A. Kanaev, Phys. Rev. B **78**, 155204 (2008).
[80] A. Alkauskas, J. L. Lyons, D. Steiauf, and C. G. Van de Walle, Phys. Rev. Lett. **109**, 267401 (2012).
[81] A. Alkauskas, B. B. Buckley, D. D. Awschalom, and C. G. Van de Walle, New J. Phys. **16**, 073026 (2014).
[82] N. Chejanovsky, M. Rezai, F. Paolucci, Y. Kim, T. Rendler, W. Rouabeh, F. Fávaro de Oliveira, P. Herlinger, A. Denisenko, S. Yang, I. Gerhart, A. Finkler, A. H. Smet, and J. Wrachtrup, Nano Lett. **16**, 7037 (2016).
[83] N. R. Jungwirth and G. D. Fuchs, Phys. Rev. Lett. **119**, 057401 (2017).
[84] S. A. Tawfik, S. Ali, M. Fronzi, M. Kianinia, T. T. Tran, C. Stampfl, I. Aharonovich, M. Toth, and M. J. Ford, Nanoscale **9**, 13575 (2017).
[85] F. Wu, A. Galatas, R. Sundararaman, D. Rocca, and Y. Ping, Phys. Rev. Mater. **1**, 071001 (2017).
[86] G. Cassabois, P. Valvin, and B. Gil, Phys. Rev. B **93**, 035207 (2016).
[87] X. Z. Du, M. R. Uddin, J. Li, J. Y. Lin, and H. X. Jiang, Appl. Phys. Lett. **110**, 092102 (2017).